

Breaking the Rate-Loss Relationship of Quantum Key Distribution with Asynchronous Two-Photon Interference

Yuan-Mei Xie,^{1,*} Yu-Shuo Lu,^{1,*} Chen-Xun Weng,¹ Xiao-Yu Cao,¹ Zhao-Ying Jia,¹ Yu Bao,¹ Yang Wang,¹ Yao Fu,² Hua-Lei Yin,^{1,†} and Zeng-Bing Chen^{1,2,‡}

¹*National Laboratory of Solid State Microstructures,
School of Physics and Collaborative Innovation Center of Advanced
Microstructures, Nanjing University, Nanjing 210093, China.*

²*MatricTime Digital Technology Co. Ltd., Nanjing 211899, China*

Twin-field quantum key distribution can overcome the repeaterless bound via single-photon interference. However, the requirements of phase-locking and phase-tracking techniques drastically increase the experimental complexity, economic cost and prohibit free-space realization. Inspired by the duality in entanglement, we herein present an asynchronous measurement-device-independent quantum key distribution protocol that can surpass the repeaterless bound even without phase locking and phase tracking. Leveraging the concept of time multiplexing, asynchronous two-photon Bell-state measurement is realized by postmatching two interference detection events. For a 1 GHz system, the new protocol reaches a transmission distance of 450 km without phase tracking. After further removing phase locking, our protocol is still capable of breaking the bound at 270 km by employing a 10 GHz system. Intriguingly, when using the same experimental techniques, our protocol has a higher key rate than the phase-matching-type twin-field protocol. In the presence of imperfect intensity modulation, it also has a significant advantage in terms of the transmission distance over the sending-or-not-sending type twin-field protocol. With high key rates and accessible technology, our work paves the way for realistic global quantum networks across space, air, and water to the ground.

I. INTRODUCTION

Quantum key distribution (QKD) [1, 2] allows the distribution of information-theoretically secure keys guaranteed by quantum mechanical limits. However, experimental implementations of QKD always deviate from the theoretical assumptions used in security proofs, leading to various quantum hacking attacks [3–7]. Fortunately, all security loopholes on the detection side are closed by measurement-device-independent QKD (MDIQKD) [8], which introduces an untrusted third party, Charlie, to perform two-photon Bell-state measurement in the intermediate node. Thus far, MDIQKD has made many theoretical and experimental breakthroughs [9–24].

However, because a significant number of photons are inevitably lost in the fiber channel, the key rate of most QKD protocols, including MDIQKD, is rigorously limited by the repeaterless bound [25–27], more precisely, the Pirandola–Laurenza–Ottaviani–Banchi (PLOB) bound $R = -\log_2(1 - \eta)$ [26], where R is the secret key rate and η is the total channel transmittance between the two users. Utilizing single-photon interference, twin-field QKD (TFQKD) [28] and its variants [29–40], such as sending-or-not-sending QKD (SNSQKD) [30] and phase-matching QKD (PMQKD) [29, 37], have been proposed to increase the key rate to $O(\sqrt{\eta})$, overcoming the PLOB bound. Since then, they have aroused widespread

concern. For example, remarkable progress has been made in the theory of finite key analysis [41–44]. Additionally, some notable experimental implementations have been reported [45–54]. The longest transmission distance of more than 600 km was recently achieved in the laboratory through optical fibers [55, 56].

Because the phase evolution of the twin fields is sensitive to both channel length drift and frequency difference between two user lasers, phase-tracking and phase-locking techniques are vital for twin-field-type protocols. Phase tracking is used to compensate for the phase noise caused by the fiber length drift, where bright reference light pulses are sent to measure the phase noise. However, the performance of the system is severely affected because the bright light causes scattering noise and occupies the time of the quantum signal [45, 47–51, 53]. Phase tracking also imposes a high counting requirement on the detectors. To address the laser frequency difference, several types of phase-locking techniques are utilized, including laser injection [17], optical phase-locked loop [57, 58], and time-frequency dissemination techniques [48, 59]. However, they all require additional channels to transfer the reference light. In addition, laser injection may introduce security risks [60, 61], and the optical phase-locked loop and the time-frequency dissemination technique both require complicated feedback systems. An ingenious replacement for phase locking and phase tracking in TFQKD experiments [46, 52] is the plug-and-play type construction [31], but it is susceptible to Trojan horse attacks [62–65]. Furthermore, free-space realization of QKD in various types of channels, including the atmosphere [66, 67], seawater [68], and satellite-to-ground channels [69–72], is essential to estab-

* These authors contributed equally to this work

† hlyin@nju.edu.cn

‡ zbchen@nju.edu.cn

lishing a global-scale quantum networks [73, 74]. However, deploying phase-locking and phase-tracking techniques, which require additional channels and erbium-doped fiber amplifiers as repeaters in classical links, is difficult in free space. Therefore, these technical requirements immensely increase experimental complexity, incur security risks, and hinder the implementation of TFQKD in commerce and networks.

In this work, we propose an asynchronous-MDIQKD protocol to remove these requirements. It has a simple hardware implementation while enjoying a high key rate. Recall that in the conventional time-bin encoding MDIQKD scheme [75], coincident detection of two neighboring time bins is required, resulting in the $O(\eta)$ scaling of the key rate [27]. Inspired by the dualism in the entanglement of identical particles [76], we observe that the two neighboring time bins can actually be decoupled. Specifically, the requirement for coincident detection of two neighboring time bins is unnecessary. By utilizing time multiplexing, we match two detected time bins that are phase-correlated to establish an asynchronous two-photon Bell state, and the key rate is enhanced to $O(\sqrt{\eta})$. This can be regarded as breaking the recently proposed linear boundary of dual-rail protocols [27]. We highlight the intrinsic differences between the time-bin encoding and the polarization encoding of MDIQKD—time multiplexing is possible solely for time-bin encoding, where there are infinite time modes. For polarization encoding, only two orthogonal modes exist.

Because the phase noise differences of each time bin are approximately equal in a short time interval, we can post-match two phase-related time bins without the phase-tracking and phase-locking techniques at the cost of a slight increase in the interference error rate. We show that after removing these techniques, the corresponding interference error rate between the two users is approximately 0.1π within $1 \mu s$ with simple commercially available instruments, giving rise to an interference error rate of approximately 2.5%. In this case, our protocol can beat the PLOB bound at a distance of approximately 270 km, achieving a reasonable trade-off between practicality and performance. Moreover, when the imperfection in light intensity modulation is considered [77], our protocol achieves a longer transmission distance and a higher key rate compared with SNSQKD with actively odd-parity pairing (AOPP) [78, 79] and PMQKD [37] when using the same experimental techniques. By circumventing the need for phase locking and phase tracking, our protocol enables quantum key distribution to break the repeaterless bound in free space.

II. ASYNCHRONOUS-MDIQKD PROTOCOL

In this section, we first introduce the basic idea of the asynchronous-MDIQKD protocol and then present a detailed protocol description.

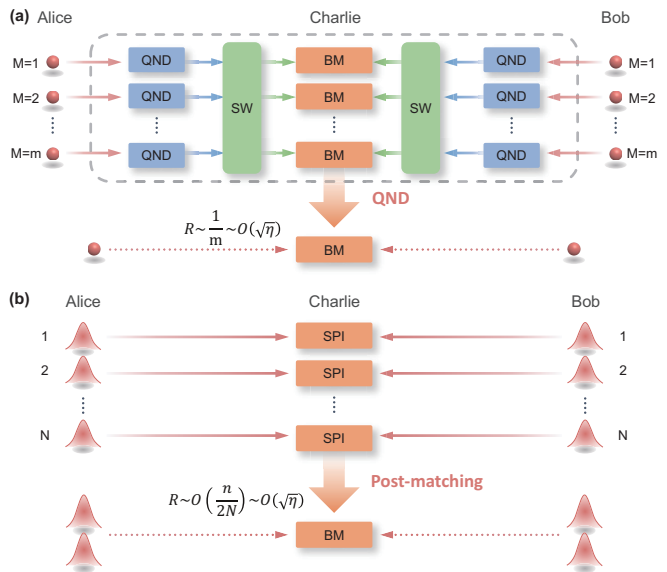


FIG. 1. Basic idea of the adaptive MDIQKD scheme [80] and this work. (a) In the adaptive MDIQKD scheme, Alice and Bob send m single-photon pulses to Charlie using spatial multiplexing. Charlie applies quantum nondemolition measurement (QND) to confirm the arrival of pulses, matches the arriving pulses using optical switches (SW), and performs two-photon Bell measurements (BM) on the pairs. (b) In our asynchronous-MDIQKD protocol, Alice and Bob send N pulses to Charlie to perform single-photon interference (SPI), and a two-photon Bell state is obtained by postmatching two successful SPI events.

A. Protocol topology

Our proposal is motivated by the spatial multiplexing adaptive MDIQKD scheme [80], as shown in Fig. 1(a). In this scheme, the idea of spatial multiplexing is leveraged, where m optical pulses in single-photon states pass through m channels. When $m\sqrt{\eta} \geq 1$, one or more single photons arrive at Charlie from Alice and Bob each, with unitary probability, resulting in $O(\sqrt{\eta})$ scaling with the key rate. One may naturally consider whether time multiplexing can be applied. Fortunately, time multiplexing is feasible with the property of entanglement dualism [76].

In the time-bin encoding MDIQKD [75], the information is encoded in the relative phase between the optical modes in two separate time bins i, j , with $i = 2t - 1$, $j = 2t$, where t is an integer. Let $|1, 0\rangle^{i,j} = |1\rangle^i |0\rangle^j$ denote the quantum state, where there is one photon in time bin i and zero photon in time bin j . Alice and Bob prepare quantum states $|+z\rangle = |1, 0\rangle^{i,j}$, $|-z\rangle = |0, 1\rangle^{i,j}$, and $|\pm x\rangle = (|1, 0\rangle^{i,j} \pm |0, 1\rangle^{i,j})/\sqrt{2}$, and send them to Charlie for Bell-state measurement, where $|\pm z\rangle$ are the eigenstates in the Z basis, and $|\pm x\rangle$ are the eigenstates in the X basis. When Charlie announces that one of the

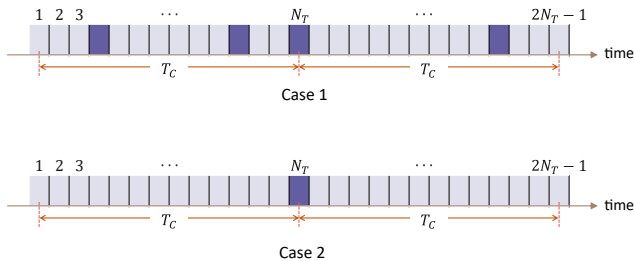


FIG. 2. Schematic of *case 1* and *case 2*. Each time bin is represented by a lattice, and detection events are painted in deep purple. *case 1*: a detection event around which other detection events can be found within T_c ; *case 2*: a detection event around which there are no other detection events within T_c . N_T is the total number of pulses sent within T_c , which is proportional to the system repetition rate.

Bell states $|\psi^\pm\rangle$ is detected, we have

$$\begin{aligned} |\psi^\pm\rangle &= \frac{1}{\sqrt{2}}(|1, 0\rangle_a^{i,j} |0, 1\rangle_b^{i,j} \pm |0, 1\rangle_a^{i,j} |1, 0\rangle_b^{i,j}) \\ &= \frac{1}{\sqrt{2}}(|1, 0\rangle_{a,b}^i |0, 1\rangle_{a,b}^j \pm |0, 1\rangle_{a,b}^i |1, 0\rangle_{a,b}^j), \end{aligned} \quad (1)$$

where subscript a represents mode ‘‘Alice’’ and b represents mode ‘‘Bob.’’ The second equation is obtained via the property of dualism in entanglement of identical particles [76]. We notice that i and j can be decoupled as two independent variables, which makes time multiplexing possible.

The basic idea of our asynchronous-MDIQKD protocol is illustrated in Fig. 1(b). N pairs of optical pulses are sent in N time bins. In each time bin, single-photon interference is performed, and $n \approx N\sqrt{\eta}$ successful detection events are obtained. Alice and Bob can post-match successful detection events of two time bins that are phase-correlated to postselect two-photon entangled states $|\psi^\pm\rangle$, leading to the $O(\sqrt{\eta})$ decay of the key rate.

We consider the case in which Alice and Bob always match two successful detection events within a short time interval T_c , where T_c is on the order of microseconds. Hereafter, we abbreviate a successful detection event to a detection event for simplicity. As shown in Fig. 2, the detection events can be classified into two cases: *case 1* and *case 2*. The *case 1* event indicates that other detection events can be found around it within T_c , and the phase noise differences of detection events in T_c are unknown but almost the same. The *case 2* event indicates that there are no other detection events around it within T_c . After removing phase tracking and phase locking, the phase noise difference of each *case 2* event becomes indeterminate. This means that *case 2* events have no phase correlations with each other. These events should be carefully handled to ensure security. For example, Charlie can know the total photon number in each optical pulse pair sent by Alice and Bob via quantum nondemolition measurements, and Charlie always lets the joint

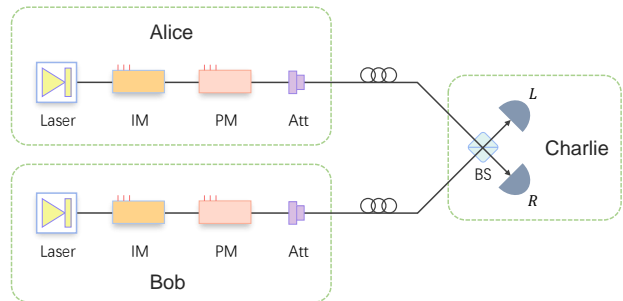


FIG. 3. Schematic of the setup for the asynchronous-MDIQKD protocol. Alice and Bob utilize a narrow-linewidth continuous-wave laser, intensity modulator (IM), phase modulator (PM), and attenuator (ATT) to prepare phase-randomized weak coherent sources with different intensities and phases. Charlie performs interference measurements with a beam splitter (BS) and single-photon detectors. Charlie announces the detection events where only the detector **L** or **R** clicks.

single-photon to be detected as *case 2* events. Charlie’s operation would not be found by Alice and Bob. If Alice and Bob discard *case 2* events, the single-photon pairs cannot be reasonably estimated using the conventional decoy-state method. Fortunately, a sufficiently small number (one on average) of *case 2* events will not affect the security of the protocol.

B. Protocol description

Schematic of the asynchronous-MDIQKD setup is shown in Fig. 3, and the details of the protocol are presented as follows.

1. *Preparation.* Alice and Bob repeat the first two steps for N rounds to obtain sufficient data. At each time bin $i \in \{1, 2, \dots, N\}$, both phase $\theta_a^i \in [0, 2\pi)$ and classical bit $r_a^i \in \{0, 1\}$ are randomly chosen by Alice. Alice then prepares a weak coherent pulse $|e^{i(\theta_a^i + r_a^i \pi)} \sqrt{k_a^i}\rangle$ with probability p_{k_a} , where $k_a^i \in \{\mu_a, \nu_a, \mathbf{o}_a, \hat{\mathbf{o}}_a\}$ corresponds to the signal, decoy, preserve-vacuum, and declare-vacuum intensities, respectively ($\mu_a > \nu_a > \mathbf{o}_a = \hat{\mathbf{o}}_a = 0$). Similarly, Bob prepares a phase-randomized weak coherent pulse. Alice and Bob send the corresponding pulses $|e^{i(\theta_a^i + r_a^i \pi)} \sqrt{k_a^i}\rangle$ and $|e^{i(\theta_b^i + r_b^i \pi)} \sqrt{k_b^i}\rangle$ ($k_b^i \in \{\mu_b, \nu_b, \mathbf{o}_b, \hat{\mathbf{o}}_b\}$) to Charlie via insecure quantum channels.

2. *Measurement.* For each time bin i , Charlie performs interference measurement on the two received pulses. Charlie obtains a detection event when only one detector clicks. He publicly announces whether a detection event is obtained and which detector clicked. In the following description, we define $\{k_a, k_b\}$ as a detection event when Alice sends intensity k_a , and Bob sends k_b . The compressed notation $\{k_a^i k_a^j, k_b^i k_b^j\}$ indicates that $\{k_a^i, k_b^i\}$ and $\{k_a^j, k_b^j\}$ are matched, the first label referring to time

bin i , and the second to time bin j .

3. *Sifting.* Alice and Bob first check the number of *case 2* events. If the number of occurrences of *case 2* is smaller than or equal to Λ , the data of *case 2* can be discarded; otherwise, they abort the protocol. For *case 1* events, when at least either Alice or Bob chooses a decoy or declare-vacuum intensity, they announce their intensities and phase information through authenticated channels. Alice and Bob then use the following rules to randomly match two *case 1* events with a time interval of less than T_c .

The unannounced detection events $\{\mu_a, \mathbf{o}_b\}$, $\{\mu_a, \mu_b\}$, $\{\mathbf{o}_a, \mu_b\}$, and $\{\mathbf{o}_a, \mathbf{o}_b\}$ are used to generate key bits in the Z basis. For these events, Alice randomly matches a time bin i of intensity μ_a with another time bin j of intensity \mathbf{o}_a . They discard detection events that cannot find a matchable peer. Then, Alice sets her bit value to 0 (1) if $i < j$ ($i > j$) and informs Bob of the serial numbers i and j . In the corresponding time bins, if Bob chooses intensities $k_b^{\min\{i,j\}} = \mu_b$ (\mathbf{o}_b) and $k_b^{\max\{i,j\}} = \mathbf{o}_b$ (μ_b), the bit value is set to 0 (1). Bob announces an event where $k_b^i = k_b^j = \mathbf{o}_b$ or μ_b . Thus, the valid events in the Z basis are $\{\mu_a \mathbf{o}_a, \mathbf{o}_b \mu_b\}$, $\{\mu_a \mathbf{o}_a, \mu_b \mathbf{o}_b\}$, $\{\mathbf{o}_a \mu_a, \mathbf{o}_b \mu_b\}$, and $\{\mathbf{o}_a \mu_a, \mu_b \mathbf{o}_b\}$.

The detection events $\{\nu_a, \nu_b\}$, $\{o_a, \nu_b\}$, $\{\nu_a, o_b\}$, $\{\hat{\mathbf{o}}_a, o_b\}$, and $\{\mathbf{o}_a, \hat{\mathbf{o}}_b\}$ are used to generate key bits in the X basis, where $o_{a(b)} \in \{\mathbf{o}_{a(b)}, \hat{\mathbf{o}}_{a(b)}\}$. The global phase of Alice (Bob) at time bin i is defined as $\varphi_{a(b)}^i := \theta_{a(b)}^i + \phi_{a(b)}^i$, where $\phi_{a(b)}^i$ is the corresponding phase noise resulted from the fiber channel. At each time bin i , Alice and Bob calculate the global phase difference $\varphi^i = \varphi_a^i - \varphi_b^i$, and randomly choose two detection events that satisfy $k_a^i = k_a^j$, $k_b^i = k_b^j$, and $|\varphi^i - \varphi^j| = 0$ or π . They then match the two events as $\{k_a^i k_a^j, k_b^i k_b^j\}$. By calculating the classical bits $r_a^i \oplus r_a^j$ and $r_b^i \oplus r_b^j$, Alice and Bob extract a bit value in the X basis, respectively. Afterwards, in the Z basis, Bob always flips his bit. In the X basis, Bob flips part of his bits to correctly correlate them with Alice's (see Table. I).

4. *Parameter estimation.* Alice and Bob exploit the random bits from the Z basis to form the n^z -length raw key bit. The remaining bits in the Z basis were used to calculate the bit error rate E^z . They reveal all bit values in the X basis to obtain the total number of errors. The decoy-state method [81, 82] was utilized to estimate the number of vacuum events in the Z basis $s_{0\mu_b}^z$, number of single-photon pairs s_{11}^z , bit error rate in the X basis e_{11}^x , and phase error rate of single-photon pairs ϕ_{11}^z in the Z basis (see Appendix A for details).

Note: To estimate the single-photon component gain of each postmatching interval, we assume that the single-photon distributions in all detection events are independent and identical.

5. *Postprocessing.* Alice and Bob distill the final keys by using the error correction algorithm with ε_{cor} -correct, and the privacy amplification algorithm with ε_{sec} -secret. Similar to Ref. [15], the length of the final secret key ℓ

with total security $\varepsilon_{\text{AMDI}} = \varepsilon_{\text{sec}} + \varepsilon_{\text{cor}}$ can be given by

$$\ell = s_{0\mu_b}^z + s_{11}^z \left[1 - H_2(\bar{\phi}_{11}^z) \right] - \lambda_{\text{EC}} - \log_2 \frac{2}{\varepsilon_{\text{cor}}} - 2 \log_2 \frac{2}{\varepsilon' \hat{\varepsilon}} - 2 \log_2 \frac{1}{2\varepsilon_{\text{PA}}}, \quad (2)$$

where \underline{x} and \bar{x} denote the lower and upper bounds of the observed value x , respectively. $\lambda_{\text{EC}} = n^z f H_2(E^z)$ is the amount of information leaked during error correction, where f is the error correction efficiency, and $H_2(x) = -x \log_2 x - (1-x) \log_2 (1-x)$ is the binary Shannon entropy function. ε_{cor} is the failure probability of error verification, and ε_{PA} refers to the failure probability of privacy amplification. ε' and $\hat{\varepsilon}$ represent the coefficients when using the chain rules of smooth min-entropy and max-entropy, respectively. $\varepsilon_{\text{sec}} = 2(\varepsilon' + \hat{\varepsilon} + 2\varepsilon_e) + \varepsilon_\beta + \varepsilon_0 + \varepsilon_1 + \varepsilon_{\text{PA}}$, where ε_0 , ε_1 and ε_e are the failure probabilities of estimating the terms $s_{0\mu_b}^z$, s_{11}^z , and ϕ_{11}^z , respectively.

III. EXPERIMENTAL DISCUSSION

In the asynchronous-MDIQKD protocol, the information in the interference mode is encoded in the phase difference of two matched time bins. One may regard the latter as the reference mode and the former as the signal mode, which is the same as the phase-encoding MDIQKD [75]. Alice and Bob postmatch pulses of two time bins i and j with phase relation $|\varphi^i - \varphi^j| = 0$ or π , where $\varphi^{i(j)} = \theta_a^{i(j)} - \theta_b^{i(j)} + \phi^{i(j)}$, $\theta_a^{i(j)}$, and $\theta_b^{i(j)}$ are random phases known to Alice and Bob. $\phi^{i(j)} = \phi_a^{i(j)} - \phi_b^{i(j)}$ is determined by the frequency difference between the two users' lasers and the fluctuation of the fiber channels. When the two pulses sent by Alice and Bob reach Charlie, the phase evolutions of the two pulses are $\phi_a^i = 2\pi v_a^i (t^i - l_a^i/s)$ and $\phi_b^i = 2\pi v_b^i (t^i - l_b^i/s)$, respectively, where t^i is the time of the time bin i , $v_{a(b)}^i$ is the laser frequency, and $l_{a(b)}^i$ is the fiber length between Alice (Bob) and Charlie at time bin i . In symmetric channels, the differential phase evolution between Alice and Bob

TABLE I. Postprocessing of raw key in the sifting step. In the X basis, Bob decides whether to implement a key bit flip to guarantee correct correlations, depending on the clicking detectors announced by Charlie and the global phase difference between two matching time bins. Here, **RL** (**LR**) denotes the detectors **R** (**L**) and **L** (**R**) clicks at time bins i and j , respectively. **RR** (**LL**) denotes that the detector **R** (**L**) clicks at time bins i and j .

Measurement results of Charlie		
Global phase difference	RL (LR)	RR (LL)
$ \varphi^i - \varphi^j = 0$	Bit flip	—
$ \varphi^i - \varphi^j = \pi$	—	Bit flip

can be expressed as

$$\phi^i = \phi_a^i - \phi_b^i = 2\pi\delta v^i t^i - \frac{2\pi}{s}(\delta v^i l^i + v^i \delta l^i), \quad (3)$$

where $\delta v^i = v_a^i - v_b^i$, $\delta l^i = l_a^i - l_b^i$, $l^i = (l_a^i + l_b^i)/2$ and $v^i = (v_a^i + v_b^i)/2$. Ensuring the phase correlation between time bins i and j is essential for postmatching. In the experiment, when the time interval for postmatching T_c is large, the phase correlation can be maintained by using phase-tracking and phase-locking techniques to measure ϕ in each time bin. Fortunately, when T_c is small, the phase correlation naturally exists, that is, ϕ is approximately constant within T_c because the fiber length drift rate and relative phase drift rate between lasers are relatively small. Therefore, our protocol can discard phase-tracking and phase-locking techniques at the cost of a slight increase in the interference error rate.

A. Removing phase tracking

Assuming that the frequencies of the two user lasers are synchronized with phase-locking techniques, $v_a^{i(j)} = v_b^{i(j)} = v^{i(j)}$, we have

$$\phi^j - \phi^i = \frac{2\pi}{s} (v^j \delta l^j - v^i \delta l^i). \quad (4)$$

When T_c is on the order of tens of microseconds, say 50 μs , the frequency drift is small for commercially available narrow-linewidth lasers. Hence, $\phi^j - \phi^i$ is mainly determined by the relative phase drift caused by the fiber length drift, which was measured to be approximately 8 rad/ms @ 402 km [49], corresponding to a phase drift of 0.4 rad per 50 μs . Note that two time bins i and j are randomly and uniformly distributed within the time interval T_c ; therefore, the mean phase drift between the two time bins is half of the maximum value. Consequently, there will be an intrinsic interference error rate of approximately $(1 - \cos 0.2)/2 \approx 1\%$.

This indicates that our protocol with short-term matching can be experimentally implemented without phase tracking when the matching interval T_c is on the order of tens of microseconds. Note that sufficient detection counts should be accumulated per T_c for postmatching. The detection count per T_c can be approximated as $T_c F(1 - e^{-\bar{\mu}\eta_d\sqrt{\eta_{\text{ch}}}})$, where F is the system frequency, η_{ch} is the channel transmittance between Alice and Bob, η_d is the detection efficiency, and $\bar{\mu}$ is the total mean photon number of Alice and Bob. At 400 km, by using a 1 GHz system with $\eta_d = 70\%$ and ultra-low loss fiber, there will be approximately 9.3 detection events per T_c if we set $\bar{\mu} = 0.5$, which is sufficient for postmatching.

B. Removing phase tracking and phase locking

We consider the case in which neither phase-tracking nor phase-locking techniques are applied. When T_c is on

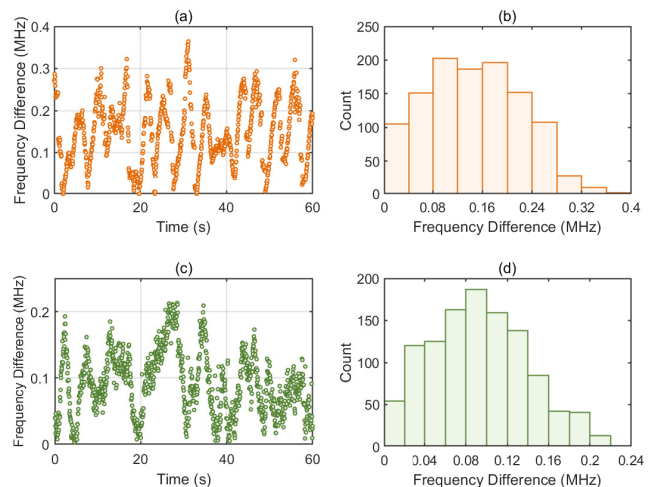


FIG. 4. Test results of the frequency difference between two independent lasers. (a) Frequency difference between two NKT lasers (E15 model) for 60 s. (b) Histogram of the frequency difference distribution between the two NKT lasers. The mean frequency difference is 0.145 MHz. (c) Frequency difference between two RIO Orion lasers of 60 s. (d) Histogram of the frequency difference distribution between two RIO Orion lasers, where the mean value is 0.0925 MHz.

the order of a few tens of microseconds, the fiber length drift is also negligible. The relative phase drift between time bins i and j is mainly determined by the frequency difference between the two independent lasers, which can be expressed as

$$\phi^j - \phi^i = 2\pi\delta v(t^j - t^i), \quad (5)$$

When pulses of time bins i and j are randomly matched, there will be an intrinsic phase misalignment $\pi\delta v T_c$. If the frequency difference is controlled to 0.1 MHz, for $T_c = 1 \mu\text{s}$, $\phi^i - \phi^j \approx 0.1\pi$ rad, resulting in an interference error rate of 2.4%. By using an experimental setup with $F = 10$ GHz (which is feasible under current technology [83, 84]) and $\eta_d = 70\%$, at 300 km, there will be approximately 11.7 detection events per 1 μs if we set $\bar{\mu} = 0.5$.

To suppress the frequency difference between two independent lasers within 0.1 MHz, one can simply measure the interference beat note frequency as a feedback signal and adjust the laser temperature. If commercially available narrow-width lasers such as the RIO Orion series or the NKT BASIK series are utilized, the laser frequency needs to be adjusted every few seconds. Additionally, if the high-finesse cavity and Pound–Drever–Hall technique are employed, the relative frequency drift can be controlled to 0.1 Hz/s [53], and the two lasers can be synchronized every tens of hours. Such experimental requirements are much easier than those of TFQKD because there is no need for time-multiplexed reference light for phase tracking and additional fiber channels for phase locking.

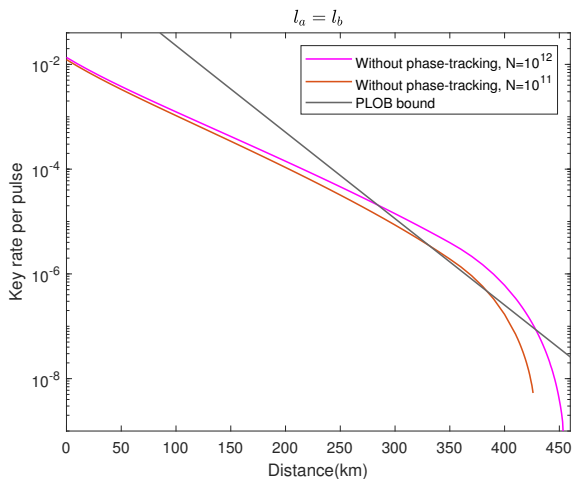


FIG. 5. Secret key rates of the asynchronous-MDIQKD with short time matching as function of the distance when implemented without phase tracking. Our protocol can break the PLOB bound at a distance of approximately 280 km with $N = 10^{12}$, and the transmission distance reaches 450 km.

We note that the experimental requirement of the asynchronous-MDIQKD protocol without phase tracking and phase locking is similar to that of the previous phase encoding MDIQKD, in which the information is encoded in the relative phase of the two time bins with delay τ . The frequency difference between the two users will inevitably misalign the phase basis, leading to intrinsic phase misalignment $\delta\phi = 2\pi\delta\nu\tau$ [22]. In experimental demonstrations in Refs. [18] and [22], the time delays are 6.37 ns and 0.5 ns, respectively. The maximum frequency difference are 37.5 MHz pm and 30 MHz, respectively, which introduce interference error rates of 0.47π and 0.03π , respectively. For our protocol with short time matching, τ is on the order of microseconds, and the frequency difference is approximately tens of kilohertz.

To demonstrate the feasibility of the experimental setup without phase-tracking and phase-locking techniques, we measured the frequency difference between two independent lasers. Two narrow-linewidth lasers working at 1550.12 nm emit continuous light, interfere with a beam splitter, and are detected by a photoelectric detector. The beat note was recorded using an oscilloscope. Fig. 4 (a) shows the beat frequencies of the two NKT lasers (Koheras BASIK E15). These lasers support fine piezoelectric tuning with a minimum tuning frequency of 20 kHz. During the test time of 60 s, we manually adjusted the frequency of one of the lasers every few seconds to minimize the observed beat frequency. A histogram of the recorded data is presented in Fig. 4(b), and the mean value is 0.145 MHz. We also measured the frequency difference between the two independent Rio lasers (Rio ORION). They were first tuned to the same frequency and kept free running during the 60 s test time. The collected data are shown in Fig. 4(c), and the histogram is shown in Fig. 4(d), with an average of 0.0925

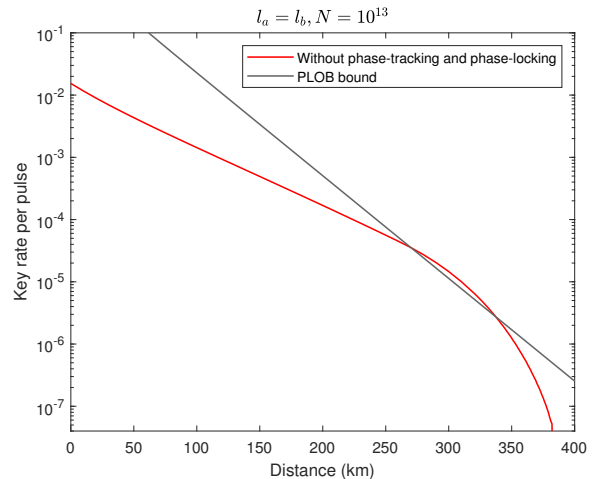


FIG. 6. Secret key rates of our protocol with short-term matching as a function of the distance where both phase-tracking and phase-locking are not adopted. Our protocol can overcome the PLOB bound at 270 km with a key rate of 2×10^{-5} .

MHz. We stress that the frequency difference can be further reduced by utilizing automatic feedback systems and improving the experimental environment.

IV. PERFORMANCE AND DISCUSSION

We numerically simulated the key rate $R = \ell/N$ of our asynchronous-MDIQKD protocol in finite-size cases. When the protocol is implemented experimentally, we set the threshold $\Lambda = 10$. The genetic algorithm is exploited to globally search for the optimal value of light intensities and their corresponding probabilities. When optimizing the key rate, we set an additional condition in which the mean number of *case 2* events $\bar{N}^{c_2} \leq 1$. Assuming that the distribution of the number of events in *case 2* follows a Poisson distribution, the probability that the observed number of *case 2* events in the experiment exceeds Λ is $1 - \sum_{k=0}^{\Lambda} \frac{\bar{N}^{c_2 k}}{k!} e^{-\bar{N}^{c_2}} \approx 1 \times 10^{-8}$, where $\bar{N}^{c_2} = \bar{N}^{c_2}$. This reveals the robustness of our protocol, which will only fail once in 100 million rounds of experiments.

The experimental parameters were set to the typical values given in Table. II. We set the failure parameters ϵ' , $\hat{\epsilon}$, ϵ_e , ϵ_β , and ϵ_{PA} to be the same ϵ . We denote the

TABLE II. Simulation parameters. η_d and p_d are the detector efficiency and dark count rate, respectively. α is the attenuation coefficient of the fiber and f denotes the error correction efficiency. ϵ is the failure probability considered in the error verification and finite data analysis processes.

η_d	p_d	α	f	ϵ
70%	10^{-8}	0.165 dB/km	1.1	$36/23 \times 10^{-10}$

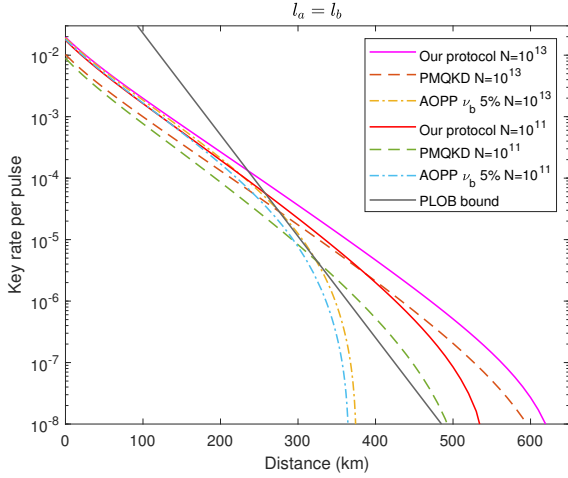


FIG. 7. Comparison of the secret key rates of the asynchronous-MDIQKD with arbitrary-time matching, PMQKD [37] and AOPP [78] in symmetric channels. The numerical results here show that our protocol has a notable advantage and is able to achieve a long transmission distance of 620 km.

distance between Alice (Bob) and Charlie as l_a (l_b). In the symmetric case, that is, $l_a = l_b = l/2$, we have $\varepsilon_0 + \varepsilon_1 = 14\varepsilon$ because the Chernoff bound [85, 86] is used 14 times to estimate $s_{0\nu_b}^z$, s_{11}^z , and e_{11}^x . The corresponding security bound is $\varepsilon_{\text{asyn}} = 2.4 \times 10^{-9}$. Similarly, in the asymmetric case, we have $\varepsilon_0 + \varepsilon_1 = 13\varepsilon$ and $\varepsilon_{\text{asyn}} = 2.3 \times 10^{-9}$.

First, we calculate the key rates of the asynchronous-MDIQKD protocol with a short time interval T_c . The detailed formulas for simulating our protocol are presented in Appendix B. The statistical fluctuation analysis formulas are presented in Appendix C. Fig. 5 shows a scenario in which phase tracking is removed. The time interval $T_c = 50 \mu\text{s}$, and the system frequency is $F = 1 \text{ GHz}$. We assume that the angle of misalignment in the X basis $\sigma = \pi/10$ rad. The key rate beats the PLOB bound at 280 km under the condition where the data size is $N = 10^{12}$ and the transmission distance reaches 450 km. One can also transmit over more than 420 km and overcome the PLOB even with a data size of $N = 10^{11}$. The key rate in the case where neither phase-tracking nor phase-locking techniques are employed is shown in Fig. 6. Here, we set $T_c = 1 \mu\text{s}$ and $F = 10 \text{ GHz}$. The simulation results show that the proposed protocol can overcome the PLOB bound at 270 km. The secure transmission distance is larger than 380 km, and the corresponding loss is 62 dB. In free space, if the Micius satellite [69] is used as the intermediate station Charlie, the key distribution between two ground nodes with a distance of approximately 1000 km can be realized. At an intercity distance of 300 km, the key rate is 0.15 Mbps, which is sufficient to perform a variety of tasks, including audio and video encryption.

For a large time interval T_c , say 1 s, the phase corre-

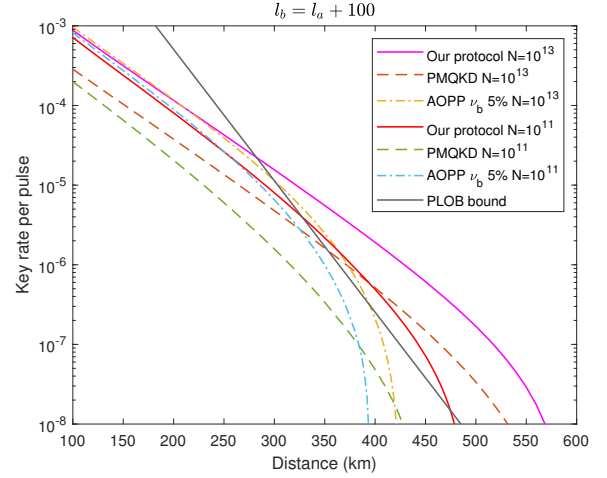


FIG. 8. Comparison of secret key rates of our protocol with arbitrary time matching, PMQKD, and AOPP versus transmission distance in asymmetric channels. Our protocol exhibits a decent performance in asymmetric channels.

lation between two time bins fades. With the same experimental complexity as TFQKD, that is, using phase locking and phase tracking, one can postmatch time bins with arbitrary time interval and achieve better performance. Here, we simulate the key rates of asynchronous-MDIQKD with arbitrary time matching and compare it with those of PMQKD (PMQKD) [37] and SNSQKD with the help of actively odd parity pairing (AOPP). We set the total number of pulses as $N = 10^{11}$ and 10^{13} , the misalignment in the X basis as $\sigma = \pi/36$, and the security bounds as $\varepsilon_{\text{AMDI}} = \varepsilon_{\text{AOPP}} = 3.6 \times 10^{-9}$ and $\varepsilon_{\text{PM}} = O(10^{-9})$. The detailed formulas for simulating our protocol are presented in Appendix B.

Because our protocol is an MDI-type protocol, the density matrix of the single-photon pair component is always identical in the X and Z bases for each user, regardless of the asymmetric source parameters chosen. This makes it possible for a dynamic quantum network to add or delete new user nodes without considering the source parameters of existing users. In contrast, to guarantee that the density matrix of the two users' joint single-photon state in the X basis is the same as that in the Z basis for SNSQKD protocols, the transmission probability and intensity of the coherent state must follow strict mathematical constraint [30, 36]. However, this constraint is difficult to realize in practice, especially in networks where users are added and deleted over time, which greatly degrades their performance. By exploiting the quantum coin concept [87, 88], a recent study provided a security proof for the SNSQKD protocol when the constraint is not satisfied [77]. When comparing the key rates, we considered that the intensity of the coherent state in AOPP does not satisfy the mathematical constraint (which is often the case in practice) with a modulation deviation of decoy state ν_b to 5%, and the other parameters have no deviation. The key rates in symmetric channels are

shown in Fig. 7. The simulation results show that the key rate of asynchronous-MDIQKD is always higher than that of PMQKD and AOPP. At 500 km, for $N = 10^{13}$, the secret key rate of our protocol is 150% higher than that of PMQKD, and the transmission distance is 240 km longer than that of AOPP. For $N = 10^{11}$, our protocol transmits over a distance of more than 500 km. Fig. 8 shows the key rate in the asymmetric channels, where $l_b = l_a + 100$ km. Notably, our protocol also performs well in asymmetric channels. At 500 km, for $N = 10^{13}$, the key rate of our protocol is 400% higher than that of PMQKD, and the transmission distance is 150 km longer than that of AOPP. Similarly, when $N = 10^{11}$, the transmission distance of the asynchronous-MDIQKD protocol is 50 km higher.

In summary, the asynchronous-MDIQKD protocol does not require complicated phase-locking and phase-tracking techniques, and it is resistant to imperfect intensity modulation. Therefore, an intercity quantum network is possible, where users can dynamically access and freely choose to perform asynchronous-MDIQKD with short time matching or arbitrary time matching.

V. CONCLUSION

In this work, inspired by dualism in entanglement, we presented an asynchronous-MDIQKD protocol through time multiplexing. We realized $O(\sqrt{\eta})$ scaling of the key rate with asynchronous two-photon interference, thus surpassing the PLOB bound. By removing phase locking and phase tracking, our protocol greatly simplifies the hardware requirement with a small sacrifice in performance. When using the same experimental techniques as TFQKD, our protocol is secure against coherent attacks, and shows longer transmission and higher key rate than PMQKD and SNSQKD (AOPP), considering imperfect intensity modulation. Our work also suggests a practical method of overcoming the linear bound of dual-rail protocols [27] without challenging technologies. In addition, our protocol can also exploit the six-state encoding [89] due to random phase modulation. Therefore, if applying single photon sources in the Z basis, our protocol can be made secure up to higher error rate by establishing the non-trivial mutual information between the bit-flip and phase error patterns [89, 90], thereby achieving a higher key rate. This work exhibits remarkable superiority in intercity quantum network deployment for balancing performance and technical complexity. We believe the key contributions of this work will produce exciting opportunities to the widespread deployment of global quantum networks beyond quantum key distribution, ranging from quantum repeaters to quantum entanglement distribution.

ACKNOWLEDGMENTS

We gratefully acknowledge the support from the National Natural Science Foundation of China (No. 61801420),

the Natural Science Foundation of Jiangsu Province (No. BK20211145), the Fundamental Research Funds for the Central Universities (No. 020414380182), the Key Research and Development Program of Nanjing Jiangbei New Area (No. ZDYD20210101), the Key-Area Research and Development Program of Guangdong Province (No. 2020B0303040001), and the China Postdoctoral Science Foundation (No. 2021M691536).

Appendix A: Simulation formulas

In this section, we calculate the parameters in Eq. (2) to estimate the secret key rate. In the following description, let x^* be the expected value of x . We denote the number of $\{k_a, k_b\}$ as $x_{k_a k_b}$. We denote the number and error number of events $\{k_a^i k_b^j, k_b^i k_a^j\}$ after postmatching as $n_{k_a^i k_b^j, k_b^i k_a^j}$ and $m_{k_a^i k_b^j, k_b^i k_a^j}$, respectively. For simplicity, we abbreviate $k_a^i k_b^j, k_b^i k_a^j$ as $2k_a, 2k_b$ when $k_a^i = k_b^j$ and $k_b^i = k_a^j$.

1. \underline{s}_{11}^z . s_{11}^z corresponds to the number of successful detection events where Alice and Bob each emit a single photon in different time bins in the Z basis. We define z_{10} (z_{01}) as the number of events in which Alice (Bob) emits a single photon and Bob (Alice) emits a vacuum state in $\{\mu_a, \mathbf{o}_b\}$ ($\{\mathbf{o}_a, \mu_b\}$) event. The lower bounds of their expected values are $\underline{z}_{10}^* = N p_{\mu_a} p_{\mathbf{o}_b} \mu_a e^{-\mu_a} \underline{y}_{10}^*$ and $\underline{z}_{01}^* = N p_{\mathbf{o}_a} p_{\mu_b} \mu_b e^{-\mu_b} \underline{y}_{01}^*$, where the yields \underline{y}_{10}^* and \underline{y}_{01}^* are the corresponding yields. These can be estimated using the decoy-state method:

$$\underline{y}_{01}^* \geq \frac{\mu_b}{N(\mu_b \nu_b - \nu_b^2)} \left(\frac{e^{\nu_b} \underline{x}_{\mathbf{o}_a \nu_b}^*}{p_{\mathbf{o}_a} p_{\nu_b}} - \frac{\nu_b^2 e^{\mu_b} \bar{x}_{\mathbf{o}_a \mu_b}^*}{\mu_b^2 p_{\mathbf{o}_a} p_{\mu_b}} - \frac{\mu_b^2 - \nu_b^2}{\mu_b^2} \frac{\bar{x}_{\mathbf{o}_o}^{d*}}{p_{\mathbf{o}_a \mathbf{o}_b}^d} \right), \quad (\text{A1})$$

$$\underline{y}_{10}^* \geq \frac{\mu_a}{N(\mu_a \nu_a - \nu_a^2)} \left(\frac{e^{\nu_a} \underline{x}_{\nu_a \mathbf{o}_b}^*}{p_{\nu_a} p_{\mathbf{o}_b}} - \frac{\nu_a^2 e^{\mu_a} \bar{x}_{\mu_a \mathbf{o}_b}^*}{\mu_a^2 p_{\mu_a} p_{\mathbf{o}_b}} - \frac{\mu_a^2 - \nu_a^2}{\mu_a^2} \frac{\bar{x}_{\mathbf{o}_o}^{d*}}{p_{\mathbf{o}_a \mathbf{o}_b}^d} \right), \quad (\text{A2})$$

where $x_{\mathbf{o}_o}^d = x_{\mathbf{o}_a \mathbf{o}_b} + x_{\mathbf{o}_a \mathbf{o}_b} + x_{\mathbf{o}_a \mathbf{o}_b}$ represents the number of events where at least one user chooses the declare-vacuum state and $p_{\mathbf{o}_o}^d = p_{\mathbf{o}_a \mathbf{o}_b} + p_{\mathbf{o}_a \mathbf{o}_b} + p_{\mathbf{o}_a \mathbf{o}_b}$ refers to the corresponding probability. Thus, the lower bound of s_{11}^{z*} can be given by

$$\underline{s}_{11}^{z*} = n_C^z \frac{\underline{z}_{10}^*}{x_{\mu_a \mathbf{o}_b}} \frac{\underline{z}_{01}^*}{x_{\mathbf{o}_a \mu_b}} = \frac{\underline{z}_{10}^* \underline{z}_{01}^*}{x_{\max}}. \quad (\text{A3})$$

where $x_0 = x_{\mathbf{o}_a \mu_b} + x_{\mathbf{o}_a \mathbf{o}_b}$, $x_1 = x_{\mu_a \mathbf{o}_b} + x_{\mu_a \mu_b}$ and $x_{\max} = \max\{x_0, x_1\}$.

2. $\underline{s}_{0\mu_b}^z$. $s_{0\mu_b}^z$ represents the number of events in the Z basis, Alice emits a zero-photon state in the two matched time bins, and the total intensity of Bob's pulses is μ_b . We define z_{00} ($z_{0\mu_b}$) as the number of detection events where the state sent by Alice collapses to the vacuum

state in the $\{\mu_a, \mathbf{o}_b\}$ ($\{\mu_a, \mu_b\}$) event. The lower bounds of the expected values are $\underline{z}_{00}^* = p_{\mu_a} p_{\mathbf{o}_b} e^{-\mu_a} \underline{x}_{\mathbf{o}_b}^{d*} / p_{\mathbf{o}_b}^d$ and $\underline{z}_{0\mu_b}^* = p_{\mu_a} p_{\mu_b} e^{-\mu_a} \underline{x}_{\mathbf{o}_a \mu_b}^* / p_{\mathbf{o}_a} p_{\mu_b}$, respectively. In this study, we employed the relation between the expected value $\underline{x}_{\mathbf{o}_a \mu_b}^* = p_{\mathbf{o}_a} \underline{x}_{\hat{\delta}_a \mu_b}^* / p_{\hat{\delta}_a}$, and $\underline{x}_{\mathbf{o}_a \mathbf{o}_b}^* = p_{\mathbf{o}_a} p_{\mathbf{o}_b} \underline{x}_{\mathbf{o}_b}^{d*} / p_{\mathbf{o}_b}^d$. The lower bound of $\underline{s}_{0\mu_b}^*$ can be written as

$$\underline{s}_{0\mu_b}^* = n_C^* \frac{\underline{z}_{00}^*}{x_{\mu_a \mathbf{o}_b}^*} + n_E^* \frac{\underline{z}_{0\mu_b}^*}{x_{\mu_a \mu_b}^*}, \quad (\text{A4})$$

3. \underline{s}_{11}^x . The phase difference between Alice and Bob is defined as $\varphi = \theta_a - \theta_b + \phi$ and the corresponding number in the $\{k_a, k_b\}$ event as $x_{k_a k_b}^\varphi$. In the post-matching step, two time bins are matched if they have the same phase difference φ , and all $\{2\nu_a, 2\nu_b\}$ events can be grouped according to the phase difference φ . We denote the number of $\{2\nu_a, 2\nu_b\}$ events with phase difference φ as $n_{2\nu_a, 2\nu_b}^\varphi = x_{2\nu_a, 2\nu_b}^\varphi / 2$. Similar to the time-bin MDIQKD, the expected yields of single-photon pairs in the X and Z bases satisfy the following relation:

$$\begin{aligned} Y_{11}^{x*} &= Y_{11}^{z*} = \frac{1}{4} (y_{01}^* y_{10}^* + y_{10}^* y_{01}^* + y_{00}^* y_{11}^* + y_{11}^* y_{00}^*) \\ &\geq \frac{1}{2} y_{10}^* y_{01}^*. \end{aligned} \quad (\text{A5})$$

Suppose the global phase difference φ is a randomly and uniformly distributed value, and the expected number of single-photon pairs can be given by

$$\begin{aligned} s_{11}^{x*} &= \frac{1}{2\pi} \int_0^{2\pi} n_{2\nu_a, 2\nu_b}^\varphi \times \frac{4\nu_a \nu_b e^{-2\nu_a - 2\nu_b}}{q_{\nu_a \nu_b}^\varphi q_{\nu_a \nu_b}^\varphi} y_{11}^{x*} d\varphi \\ &\geq \frac{1}{2\pi} \int_0^{2\pi} n_{2\nu_a, 2\nu_b}^\varphi \times \frac{\nu_a \nu_b e^{-2\nu_a - 2\nu_b}}{q_{\nu_a \nu_b}^\varphi q_{\nu_a \nu_b}^\varphi} 2y_{10}^* y_{01}^* d\varphi \\ &= N p_{\nu_a} p_{\nu_b} \nu_a \nu_b e^{-2(\nu_a + \nu_b)} y_{10}^* y_{01}^* \int_0^{2\pi} \frac{1}{2\pi q_{\nu_a \nu_b}^\varphi} d\varphi, \end{aligned} \quad (\text{A6})$$

where the coefficient 4 on the first line of the formula corresponds to the four modes of single-photon pairs in the X basis, $q_{\nu_a \nu_b}^\varphi$ is the gain when Alice chooses intensity ν_a , and Bob chooses intensity ν_b with phase difference φ and $n_{2\nu_a, 2\nu_b}^\varphi = N p_{\nu_a} p_{\nu_b} q_{\nu_a \nu_b}^\varphi / 2$. We define $q_{k_a k_b} = 1 / (2\pi) \int_0^{2\pi} q_{k_a k_b}^\varphi d\varphi$ as the average gain, given that Alice chooses intensity k_a , and Bob chooses intensity k_b . When ν_a and $\nu_b \approx 0$, there is an approximation relation $\int_0^{2\pi} 1 / (2\pi q_{\nu_a \nu_b}^\varphi) d\varphi \approx 1 / q_{\nu_a \nu_b}$.

In the discrete case, the phase difference φ is divided into M slices $\{\delta_m\}$ for $1 \leq m \leq M$, where m is an integer, where $\delta_m = [2\pi(m-1)/M, 2\pi m/M)$. The expected number of single-photon pairs is given by

$$\underline{s}_{11}^{x*} \geq \sum_{m=1}^M n_{2\nu_a, 2\nu_b}^m \times 2 \frac{\nu_a e^{-\nu_a - \nu_b} y_{10}^*}{q_{\nu_a \nu_b}^m} \frac{\nu_b e^{-\nu_a - \nu_b} y_{01}^*}{q_{\nu_a \nu_b}^m}, \quad (\text{A7})$$

where $n_{2\nu_a, 2\nu_b}^m$ is the number of $\{2\nu_a, 2\nu_b\}$ events with phase difference φ falling into slice δ_m . $q_{\nu_a \nu_b}^m$ is the corresponding gain.

4. \bar{e}_{11}^x . For single-photon pairs, the expected value of the phase error rate in the Z basis equals the expected value of the bit error rate in the X basis, and the error rate $\bar{e}_{11}^x = \bar{t}_{11}^x / \underline{s}_{11}^x$. Therefore, we first calculate the number of errors of the single-photon pairs in the X basis t_{11}^x . The upper bound of t_{11}^x can be expressed as

$$\bar{t}_{11}^x \leq m_{2\nu_a, 2\nu_b} - (m_{0, 2\nu_b} + m_{2\nu_a, 0}) + \bar{m}_{0,0}, \quad (\text{A8})$$

where $m_{0, 2\nu_b}$ ($m_{2\nu_a, 0}$) is the error count when the state sent by Alice (Bob) collapses to the vacuum state in events $\{2\nu_a, 2\nu_b\}$, and $m_{0,0}$ corresponds to the event where the states sent by Alice and Bob both collapse to vacuum states in events $\{2\nu_a, 2\nu_b\}$. The expected error counts $m_{0, 2\nu_b}^*$ and $m_{2\nu_a, 0}^*$ can be expressed as follows:

$$\begin{aligned} m_{0, 2\nu_b}^* &= e_o \frac{1}{2\pi} \int_0^{2\pi} n_{2\nu_a, 2\nu_b}^\varphi \frac{e^{-\nu_a} q_{0\nu_b}^*}{q_{\nu_a \nu_b}^\varphi} \frac{e^{-\nu_a} q_{0\nu_b}^*}{q_{\nu_a \nu_b}^\varphi} d\varphi \\ &= e_o N p_{\nu_a} p_{\nu_b} e^{-2\nu_a} q_{0\nu_b}^{*2} \frac{1}{4\pi} \int_0^{2\pi} \frac{1}{q_{\nu_a \nu_b}^\varphi} d\varphi, \\ m_{2\nu_a, 0}^* &= e_o \frac{1}{2\pi} \int_0^{2\pi} n_{2\nu_a, 2\nu_b}^\varphi \frac{e^{-\nu_b} q_{\nu_a 0}^*}{q_{\nu_a \nu_b}^\varphi} \frac{e^{-\nu_b} q_{\nu_a 0}^*}{q_{\nu_a \nu_b}^\varphi} d\varphi \\ &= e_o N p_{\nu_a} p_{\nu_b} e^{-2\nu_b} q_{\nu_a 0}^{*2} \frac{1}{4\pi} \int_0^{2\pi} \frac{1}{q_{\nu_a \nu_b}^\varphi} d\varphi, \end{aligned} \quad (\text{A9})$$

respectively, where $e_o = 1/2$ is the error rate of the background noise.

In the symmetric case, $\nu_a = \nu_b$, $p_{\mathbf{o}_a} = p_{\mathbf{o}_b}$, and $p_{\nu_a} = p_{\nu_b}$. In this case, we have $q_{\nu_a \mathbf{o}_b}^* = q_{\mathbf{o}_a \nu_b}^* = (x_{\mathbf{o}_a \nu_b} + x_{\nu_a \mathbf{o}_b})^* / (2N p_{\mathbf{o}_a} p_{\nu_b})$. In the asymmetric case, $q_{\nu_a \mathbf{o}_b}^* = x_{\nu_a \mathbf{o}_b}^* / (N p_{\nu_a} p_{\mathbf{o}_b})$ and $q_{\mathbf{o}_a \nu_b}^* = x_{\mathbf{o}_a \nu_b}^* / (N p_{\mathbf{o}_a} p_{\nu_b})$. Then, the lower bound of the observed value of $m_{0, 2\nu_b} + m_{2\nu_a, 0}$ can be written as

$$\underline{m}_{0, 2\nu_b} + \underline{m}_{2\nu_a, 0} = \varphi^L (\underline{m}_{0, 2\nu_b}^* + \underline{m}_{2\nu_a, 0}^*, \epsilon). \quad (\text{A10})$$

where $\varphi^L(x)$ is the lower bounds when using Chernoff bound to estimate the real values according to the expected values and is defined in Eq. C1. The expected value of $m_{0,0}$ can be given by

$$\begin{aligned} m_{0,0}^* &= e_o \frac{1}{2\pi} \int_0^{2\pi} n_{2\nu_a, 2\nu_b}^\varphi \frac{e^{-\nu_a - \nu_b} q_{00}^*}{q_{\nu_a \nu_b}^\varphi} \frac{e^{-\nu_a - \nu_b} q_{00}^*}{q_{\nu_a \nu_b}^\varphi} d\varphi \\ &= e_o N p_{\nu_a} p_{\nu_b} e^{-2(\nu_a + \nu_b)} q_{00}^{*2} \frac{1}{4\pi} \int_0^{2\pi} \frac{1}{q_{\nu_a \nu_b}^\varphi} d\varphi. \end{aligned} \quad (\text{A11})$$

We denote the total number of errors in events $\{2\hat{\delta}_a, 2\mathbf{o}_b\}$ and $\{2\mathbf{o}_a, 2\hat{\delta}_b\}$ as $m_{2\mathbf{o}_a, 2\mathbf{o}_b}^d$. The upper bound of q_{00}^* can be obtained from $\bar{q}_{00}^* = \bar{m}_{2\mathbf{o}_a, 2\mathbf{o}_b}^d / (N p_{\mathbf{o}_a}^d)$. The upper bound of $m_{0,0}$ can be obtained by $\bar{m}_{0,0} = \varphi^U(x) (\bar{m}_{0,0}^*, \epsilon)$, where $\varphi^U(x)$ is the upper bound while using the Chernoff bound to estimate the observed values according to the expected values and is defined in Eq. C2.

5. $\bar{\phi}_{11}^z$. Finally, for a failure probability ϵ , the upper bound of the phase error rate $\bar{\phi}_{11}^z$ can be obtained by using random sampling without replacement in Eq. (C5)

$$\bar{\phi}_{11}^z \leq \bar{e}_{11}^x + \gamma (\underline{s}_{11}^z, \underline{s}_{11}^x, \bar{e}_{11}^x, \epsilon). \quad (\text{A12})$$

Appendix B: Simulation details

1. Asynchronous-MDIQKD protocol for arbitrary-time matching

Similar to the time-bin encoding MDIQKD, the valid events after postmatching in the Z basis can be divided into correct events $\{\mu_a \mathbf{o}_a, \mathbf{o}_b \mu_b\}$, $\{\mathbf{o}_a \mu_a, \mu_b \mathbf{o}_b\}$, and incorrect events $\{\mu_a \mathbf{o}_a, \mu_b \mathbf{o}_b\}$, $\{\mathbf{o}_a \mu_a, \mathbf{o}_b \mu_b\}$. The corresponding numbers are denoted as n_C^z and n_E^z , respectively, which can be written as

$$n_C^z = x_{\min} \frac{x_{\mathbf{o}_a \mu_b} x_{\mu_a \mathbf{o}_b}}{x_0 x_1} = \frac{x_{\mathbf{o}_a \mu_b} x_{\mu_a \mathbf{o}_b}}{x_{\max}},$$

and

$$n_E^z = x_{\min} \frac{x_{\mathbf{o}_a \mathbf{o}_b} x_{\mu_a \mu_b}}{x_0 x_1} = \frac{x_{\mathbf{o}_a \mathbf{o}_b} x_{\mu_a \mu_b}}{x_{\max}},$$

where $x_{\min} = \min\{x_0, x_1\}$. The overall number of events in the Z basis is $n^z = n_C^z + n_E^z$ and the bit error rate in the Z basis is $E^z = n_E^z/n^z$.

In the X basis, the data are composed of events $\{2\nu_a, 2\nu_b\}$, $\{2\mathbf{o}_a, 2\nu_b\}$, $\{2\nu_a, 2\mathbf{o}_b\}$, $\{2\mathbf{o}_a, 2\mathbf{o}_b\}$, and $\{2\mathbf{O}_a, 2\mathbf{O}_b\}$. Without loss of generality, we consider the case in which all matched events satisfy $\theta_a^i - \theta_b^j - (\theta_a^i - \theta_b^j) + (\phi^i - \phi^j) = 0$. In this case, when $r_a^i \oplus r_b^j \oplus r_a^i \oplus r_b^j = 0$ (1), the $\{\nu_a^i \nu_a^j, \nu_b^i \nu_b^j\}$ event is considered to be an error event when different detectors (the same detector) click at time bins i and j .

When Alice and Bob send intensities k_a and k_b with phase difference φ , the gain corresponding to only one detector click is

$$\begin{aligned} q_{k_a k_b}^{L\varphi} &= y_{k_a k_b} [e^{\omega_{k_a k_b} \cos \varphi} - y_{k_a k_b}], \\ q_{k_a k_b}^{R\varphi} &= y_{k_a k_b} [e^{-\omega_{k_a k_b} \cos \varphi} - y_{k_a k_b}]. \end{aligned} \quad (\text{B1})$$

where $y_{k_a k_b} := e^{-\frac{(\eta_a k_a + \eta_b k_b)}{2}} (1 - pd)$, $\omega_{k_a k_b} := \sqrt{\eta_a k_a \eta_b k_b}$, $\eta_a = \eta_d 10^{-\alpha_a/10}$ and $\eta_b = \eta_d 10^{-\alpha_b/10}$. The overall gain can be given by $q_{k_a k_b} = 1/2\pi \int_0^{2\pi} q_{k_a k_b}^\varphi d\varphi = 1/2\pi \int_0^{2\pi} (q_{k_a k_b}^{L\varphi} + q_{k_a k_b}^{R\varphi}) d\varphi = 2y_{k_a k_b} [I_0(\omega_{k_a k_b}) - y_{k_a k_b}]$, where $I_0(x)$ represents the zero-order modified Bessel function of the first kind. The total number of $\{k_a, k_b\}$ is $x_{k_a k_b} = N p_{k_a} p_{k_b} q_{k_a k_b}$.

The overall error count in the X basis can be given as

$$\begin{aligned} m_{2\nu_a, 2\nu_b} &= \frac{1}{2\pi} \int_0^{2\pi} n_{2\nu_a, 2\nu_b}^\varphi \left[\frac{q_{\nu_a \nu_b}^{L\varphi} q_{\nu_a \nu_b}^{R(\varphi+\sigma)} + q_{\nu_a \nu_b}^{R\varphi} q_{\nu_a \nu_b}^{L(\varphi+\sigma)}}{q_{\nu_a \nu_b}^\varphi q_{\nu_a \nu_b}^{\varphi+\sigma}} \right] d\varphi \\ &= N p_{\nu_a} p_{\nu_b} \frac{1}{4\pi} \int_0^{2\pi} \frac{q_{\nu_a \nu_b}^{L\varphi} q_{\nu_a \nu_b}^{R(\varphi+\sigma)} + q_{\nu_a \nu_b}^{R\varphi} q_{\nu_a \nu_b}^{L(\varphi+\sigma)}}{q_{\nu_a \nu_b}^{\varphi+\sigma}} d\varphi. \end{aligned} \quad (\text{B2})$$

where σ refers to the angle of misalignment in the X basis.

2. Asynchronous-MDIQKD protocol for short-term matching

The total number of time bins per T_c is $N_{T_c} = T_c F$. For each detection event, the probability that it belongs to *case 1* is $p_{c_1} = 1 - (1 - \bar{p})^{2N_{T_c} - 2}$ and the probability of belonging to *case 2* is $p_{c_2} = (1 - \bar{p})^{2N_{T_c} - 2}$, where $\bar{p} = \sum_{k_a, k_b} p_{k_a} p_{k_b} q_{k_a k_b}$ is the average detection probability, and $2N_{T_c} - 2$ is the total number of time bins neighboring the given detection event. The mean number of *case 2* events is $\bar{N}^{c_2} = N p_{c_2} \bar{p}$.

For simplicity, we divide the post-matching window into d windows with a time length of T_c , where $d = N/N_{T_c}$. In the Z basis, given that Alice sends k_a and Bob sends k_b , the detection count in the i -th window and the total detection count are $x_{k_a k_b}^i = N_{T_c} p_{c_1} p_{k_a} p_{k_b} q_{k_a k_b}$ and $x_{k_a k_b} = N p_{c_1} p_{k_a} p_{k_b} q_{k_a k_b}$, respectively. After post-matching, the number of correct and incorrect events in the Z basis is

$$\begin{aligned} n_C^z &= \sum_{i=1}^d x_{\min}^i \frac{x_{\mathbf{o}_a \mu_b}^i x_{\mu_a \mathbf{o}_b}^i}{x_0^i x_1^i} = \sum_{i=1}^d \frac{x_{\mathbf{o}_a \mathbf{o}_b}^i x_{\mu_a \mu_b}^i}{x_{\max}^i}, \\ n_E^z &= \sum_{i=1}^d x_{\min}^i \frac{x_{\mathbf{o}_a \mathbf{o}_b}^i x_{\mu_a \mu_b}^i}{x_0^i x_1^i} = \sum_{i=1}^d \frac{x_{\mathbf{o}_a \mathbf{o}_b}^i x_{\mu_a \mu_b}^i}{x_{\max}^i}, \end{aligned}$$

respectively, where $x_0^i = x_{\mathbf{o}_a \mu_b}^i + x_{\mathbf{o}_a \mathbf{o}_b}^i$, $x_1^i = x_{\mu_a \mathbf{o}_b}^i + x_{\mu_a \mu_b}^i$, $x_{\min}^i = \min\{x_0^i, x_1^i\}$, $x_{\max}^i = \max\{x_0^i, x_1^i\}$. The overall number of events in the Z basis is $n^z = n_C^z + n_E^z$, and the bit error rate in the Z basis is $E^z = n_E^z/n^z$.

In our simulation, we set $M = 16$. Assuming that $x_{\nu_a \nu_b}^m$, the detection count of $\{\nu_a, \nu_b\}$ events in slice δ_m follows the Poisson distribution $P_r(x_{\nu_a \nu_b}^m = j) = \frac{\lambda^j}{j!} e^{-\lambda}$, where $\lambda = \bar{x}_{\nu_a \nu_b}^m$ is the mean value of $x_{\nu_a \nu_b}^m$. In the post-matching step, if $x_{\nu_a \nu_b}^m$ is even, all $\{\nu_a, \nu_b\}$ events within the m -th T_c will be utilized. If $x_{\nu_a \nu_b}^m$ is odd, there will be a redundant $\{\nu_a, \nu_b\}$ event to be aborted. Therefore, the mean number of $\{2\nu_a, 2\nu_b\}$ events per T_c is

$$\begin{aligned} n_{2\nu_a, 2\nu_b}^i &= \frac{2}{M} \left[\sum_k^{\lfloor \frac{N_{T_c} - 1}{2} \rfloor} k P_r(2k) + k P_r(2k + 1) \right] \\ &= \frac{1}{M} \left[\lambda - \frac{1 - e^{-2\lambda}}{2} \right]. \end{aligned} \quad (\text{B3})$$

The overall error count in the X basis can be given as

$$m_{2\nu_a, 2\nu_b}^i = n_{2\nu_a, 2\nu_b}^i \sum_{m=0}^{\frac{M}{2} - 1} \left[\frac{2}{M} \frac{q_{\nu_a \nu_b}^{L\varphi_m} q_{\nu_a \nu_b}^{R(\varphi_m + \sigma)} + q_{\nu_a \nu_b}^{R\varphi_m} q_{\nu_a \nu_b}^{L(\varphi_m + \sigma)}}{q_{\nu_a \nu_b}^{\varphi_m} q_{\nu_a \nu_b}^{\varphi_m + \sigma}} \right], \quad (\text{B4})$$

where $\varphi_m = 2\pi m/M$.

Appendix C: Statistical fluctuation analysis

In this Appendix, we introduce the statistical fluctuation analysis method [86] used in the simulation.

Chernoff bound. Let x^* be the expected value of x . For a given expected value x^* , the Chernoff bound can be used to obtain the upper and lower bounds of the observed value.

$$\bar{x} = \varphi^U(x^*) = x^* + \frac{\beta}{2} + \sqrt{2\beta x^* + \frac{\beta^2}{4}}, \quad (\text{C1})$$

and

$$\underline{x} = \varphi^L(x^*) = x^* - \sqrt{2\beta x^*}, \quad (\text{C2})$$

where $\beta = \ln \varepsilon^{-1}$.

Variant of Chernoff bound. For a given observed value x and failure probability ε , the upper and lower bounds of x^* can be acquired by the variant of the Chernoff bound

$$\bar{x}^* = x + \beta + \sqrt{2\beta x + \beta^2}, \quad (\text{C3})$$

and

$$\underline{x}^* = \max \left\{ x - \frac{\beta}{2} - \sqrt{2\beta x + \frac{\beta^2}{4}}, 0 \right\}. \quad (\text{C4})$$

Random sampling without replacement. Let $X_{n+k} := \{x_1, x_2, \dots, x_{n+k}\}$ be a string of binary bits of size $n+k$, where the number of bits is unknown. Let X_k be a random sample (without replacement) bit string with k is picked from X_{n+k} . Let λ be the probability of a bit value 1 observed in X_k . Let X_n be the remaining bit string, where the probability of bit value 1 observed in X_n is χ . The upper bound of χ can be expressed as

$$\bar{\chi} \leq \lambda + \gamma^U(n, k, \lambda, \varepsilon), \quad (\text{C5})$$

where

$$\gamma^U(n, k, \lambda, \varepsilon) = \frac{\frac{(1-2\lambda)AG}{n+k} + \sqrt{\frac{A^2G^2}{(n+k)^2} + 4\lambda(1-\lambda)G}}{2 + 2\frac{A^2G}{(n+k)^2}}, \quad (\text{C6})$$

with $A = \max\{n, k\}$ and $G = \frac{n+k}{nk} \ln \frac{n+k}{2\pi nk\lambda(1-\lambda)\varepsilon^2}$.

-
- [1] C. H. Bennett and G. Brassard, Quantum cryptography: Public key distribution and coin tossing, *Theor. Comput. Sci.* **560**, 7 (2014).
- [2] A. K. Ekert, Quantum cryptography based on bell's theorem, *Phys. Rev. Lett.* **67**, 661 (1991).
- [3] Y. Zhao, C.-H. F. Fung, B. Qi, C. Chen, and H.-K. Lo, Quantum hacking: Experimental demonstration of time-shift attack against practical quantum-key-distribution systems, *Phys. Rev. A* **78**, 042333 (2008).
- [4] L. Lydersen, C. Wiechers, C. Wittmann, D. Elser, J. Skaar, and V. Makarov, Hacking commercial quantum cryptography systems by tailored bright illumination, *Nat. Photonics* **4**, 686 (2010).
- [5] Y.-L. Tang, H.-L. Yin, X. Ma, C.-H. F. Fung, Y. Liu, H.-L. Yong, T.-Y. Chen, C.-Z. Peng, Z.-B. Chen, and J.-W. Pan, Source attack of decoy-state quantum key distribution using phase information, *Phys. Rev. A* **88**, 022308 (2013).
- [6] F. Xu, X. Ma, Q. Zhang, H.-K. Lo, and J.-W. Pan, Secure quantum key distribution with realistic devices, *Rev. Mod. Phys.* **92**, 025002 (2020).
- [7] S. Pirandola, U. L. Andersen, L. Banchi, M. Berta, D. Bunandar, R. Colbeck, D. Englund, T. Gehring, C. Lupo, C. Ottaviani, *et al.*, Advances in quantum cryptography, *Adv. Opt. Photon.* **12**, 1012 (2020).
- [8] H.-K. Lo, M. Curty, and B. Qi, Measurement-device-independent quantum key distribution, *Phys. Rev. Lett.* **108**, 130503 (2012).
- [9] S. L. Braunstein and S. Pirandola, Side-channel-free quantum key distribution, *Phys. Rev. Lett.* **108**, 130502 (2012).
- [10] Y. Liu, T.-Y. Chen, L.-J. Wang, H. Liang, G.-L. Shentu, J. Wang, K. Cui, H.-L. Yin, N.-L. Liu, L. Li, X. Ma, J. S. Pelc, M. M. Fejer, C.-Z. Peng, Q. Zhang, and J.-W. Pan, Experimental measurement-device-independent quantum key distribution, *Phys. Rev. Lett.* **111**, 130502 (2013).
- [11] A. Rubenok, J. A. Slater, P. Chan, I. Lucio-Martinez, and W. Tittel, Real-world two-photon interference and proof-of-principle quantum key distribution immune to detector attacks, *Phys. Rev. Lett.* **111**, 130501 (2013).
- [12] Y.-H. Zhou, Z.-W. Yu, and X.-B. Wang, Making the decoy-state measurement-device-independent quantum key distribution practically useful, *Phys. Rev. A* **93**, 042324 (2016).
- [13] Z. Tang, Z. Liao, F. Xu, B. Qi, L. Qian, and H.-K. Lo, Experimental demonstration of polarization encoding measurement-device-independent quantum key distribution, *Phys. Rev. Lett.* **112**, 190503 (2014).
- [14] Y. Fu, H.-L. Yin, T.-Y. Chen, and Z.-B. Chen, Long-distance measurement-device-independent multiparty quantum communication, *Phys. Rev. Lett.* **114**, 090501 (2015).
- [15] M. Curty, F. Xu, W. Cui, C. C. W. Lim, K. Tamaki, and H.-K. Lo, Finite-key analysis for measurement-device-independent quantum key distribution, *Nature Commun.* **5**, 3732 (2014).
- [16] H.-L. Yin, W.-F. Cao, Y. Fu, Y.-L. Tang, Y. Liu, T.-Y. Chen, and Z.-B. Chen, Long-distance measurement-device-independent quantum key distribution with coherent-state superpositions, *Opt. Lett.* **39**, 5451 (2014).
- [17] L. Comandar, M. Lucamarini, B. Fröhlich, J. Dynes, A. Sharpe, S.-B. Tam, Z. Yuan, R. Penty, and A. Shields, Quantum key distribution without detector vulnerabilities using optically seeded lasers, *Nat. Photonics* **10**, 312 (2016).
- [18] H.-L. Yin, T.-Y. Chen, Z.-W. Yu, H. Liu, L.-X. You, Y.-H. Zhou, S.-J. Chen, Y. Mao, M.-Q. Huang, W.-J. Zhang, H. Chen, M. J. Li, D. Nolan, F. Zhou, X. Jiang, Z. Wang,

- Q. Zhang, X.-B. Wang, and J.-W. Pan, Measurement-device-independent quantum key distribution over a 404 km optical fiber, *Phys. Rev. Lett.* **117**, 190501 (2016).
- [19] H. Semenenko, P. Sibson, A. Hart, M. G. Thompson, J. G. Rarity, and C. Erven, Chip-based measurement-device-independent quantum key distribution, *Optica* **7**, 238 (2020).
- [20] H.-L. Yin, W.-L. Wang, Y.-L. Tang, Q. Zhao, H. Liu, X.-X. Sun, W.-J. Zhang, H. Li, I. V. Puthoor, L.-X. You, *et al.*, Experimental measurement-device-independent quantum digital signatures over a metropolitan network, *Phys. Rev. A* **95**, 042338 (2017).
- [21] K. Wei, W. Li, H. Tan, Y. Li, H. Min, W.-J. Zhang, H. Li, L. You, Z. Wang, X. Jiang, *et al.*, High-speed measurement-device-independent quantum key distribution with integrated silicon photonics, *Phys. Rev. X* **10**, 031030 (2020).
- [22] R. I. Woodward, Y. Lo, M. Pittaluga, M. Minder, T. Paräiso, M. Lucamarini, Z. Yuan, and A. Shields, Gigahertz measurement-device-independent quantum key distribution using directly modulated lasers, *npj Quantum Inf.* **7** (2021).
- [23] C. Wang, Z.-Q. Yin, S. Wang, W. Chen, G.-C. Guo, and Z.-F. Han, Measurement-device-independent quantum key distribution robust against environmental disturbances, *Optica* **4**, 1016 (2017).
- [24] X. Zheng, P. Zhang, R. Ge, L. Lu, G. He, Q. Chen, F. Qu, L. Zhang, X. Cai, Y. Lu, S. Zhu, P. Wu, and X.-S. Ma, Heterogeneously integrated, superconducting silicon-photonics platform for measurement-device-independent quantum key distribution, *Adv. Photonics* **3**, 055002 (2021).
- [25] M. Takeoka, S. Guha, and M. M. Wilde, Fundamental rate-loss tradeoff for optical quantum key distribution, *Nat. Commun.* **5**, 5235 (2014).
- [26] S. Pirandola, R. Laurenza, C. Ottaviani, and L. Banchi, Fundamental limits of repeaterless quantum communications, *Nat. Commun.* **8**, 15043 (2017).
- [27] S. Das, S. Bäuml, M. Winczewski, and K. Horodecki, Universal limitations on quantum key distribution over a network, *Phys. Rev. X* **11**, 041016 (2021).
- [28] M. Lucamarini, Z. L. Yuan, J. F. Dynes, and A. J. Shields, Overcoming the rate–distance limit of quantum key distribution without quantum repeaters, *Nature* **557**, 400 (2018).
- [29] X. Ma, P. Zeng, and H. Zhou, Phase-matching quantum key distribution, *Phys. Rev. X* **8**, 031043 (2018).
- [30] X.-B. Wang, Z.-W. Yu, and X.-L. Hu, Twin-field quantum key distribution with large misalignment error, *Phys. Rev. A* **98**, 062323 (2018).
- [31] H.-L. Yin and Y. Fu, Measurement-device-independent twin-field quantum key distribution, *Sci. Rep.* **9**, 3045 (2019).
- [32] J. Lin and N. Lütkenhaus, Simple security analysis of phase-matching measurement-device-independent quantum key distribution, *Phys. Rev. A* **98**, 042332 (2018).
- [33] M. Curty, K. Azuma, and H.-K. Lo, Simple security proof of twin-field type quantum key distribution protocol, *npj Quantum Inf.* **5**, 64 (2019).
- [34] C. Cui, Z.-Q. Yin, R. Wang, W. Chen, S. Wang, G.-C. Guo, and Z.-F. Han, Twin-field quantum key distribution without phase postselection, *Phys. Rev. Applied* **11**, 034053 (2019).
- [35] H.-L. Yin and Z.-B. Chen, Coherent-state-based twin-field quantum key distribution, *Sci. Rep.* **9**, 14918 (2019).
- [36] X.-L. Hu, C. Jiang, Z.-W. Yu, and X.-B. Wang, Sending-or-not-sending twin-field protocol for quantum key distribution with asymmetric source parameters, *Phys. Rev. A* **100**, 062337 (2019).
- [37] P. Zeng, W. Wu, and X. Ma, Symmetry-protected privacy: beating the rate-distance linear bound over a noisy channel, *Phys. Rev. Applied* **13**, 064013 (2020).
- [38] Y.-M. Xie, B.-H. Li, Y.-S. Lu, X.-Y. Cao, W.-B. Liu, H.-L. Yin, and Z.-B. Chen, Overcoming the rate–distance limit of device-independent quantum key distribution, *Opt. Lett.* **46**, 1632 (2021).
- [39] R. Wang, Z.-Q. Yin, F.-Y. Lu, S. Wang, W. Chen, C.-M. Zhang, W. Huang, B.-J. Xu, G.-C. Guo, and Z.-F. Han, Optimized protocol for twin-field quantum key distribution, *Commun. Phys.* **3**, 149 (2020).
- [40] B.-H. Li, Y.-M. Xie, Z. Li, C.-X. Weng, C.-L. Li, H.-L. Yin, and Z.-B. Chen, Long-distance twin-field quantum key distribution with entangled sources, *Opt. Lett.* **46**, 5529 (2021).
- [41] K. Maeda, T. Sasaki, and M. Koashi, Repeaterless quantum key distribution with efficient finite-key analysis overcoming the rate-distance limit, *Nat. Commun.* **10**, 3140 (2019).
- [42] H.-L. Yin and Z.-B. Chen, Finite-key analysis for twin-field quantum key distribution with composable security, *Sci. Rep.* **9**, 17113 (2019).
- [43] C. Jiang, Z.-W. Yu, X.-L. Hu, and X.-B. Wang, Unconditional security of sending or not sending twin-field quantum key distribution with finite pulses, *Phys. Rev. Applied* **12**, 024061 (2019).
- [44] G. Currás-Lorenzo, Á. Navarrete, K. Azuma, G. Kato, M. Curty, and M. Razavi, Tight finite-key security for twin-field quantum key distribution, *npj Quantum Inf.* **7**, 22 (2021).
- [45] M. Minder, M. Pittaluga, G. Roberts, M. Lucamarini, J. Dynes, Z. Yuan, and A. Shields, Experimental quantum key distribution beyond the repeaterless secret key capacity, *Nat. Photonics* **13**, 334 (2019).
- [46] X. Zhong, J. Hu, M. Curty, L. Qian, and H.-K. Lo, Proof-of-principle experimental demonstration of twin-field type quantum key distribution, *Phys. Rev. Lett.* **123**, 100506 (2019).
- [47] S. Wang, D.-Y. He, Z.-Q. Yin, F.-Y. Lu, C.-H. Cui, W. Chen, Z. Zhou, G.-C. Guo, and Z.-F. Han, Beating the fundamental rate-distance limit in a proof-of-principle quantum key distribution system, *Phys. Rev. X* **9**, 021046 (2019).
- [48] Y. Liu, Z.-W. Yu, W. Zhang, J.-Y. Guan, J.-P. Chen, C. Zhang, X.-L. Hu, H. Li, C. Jiang, J. Lin, T.-Y. Chen, L. You, Z. Wang, X.-B. Wang, Q. Zhang, and J.-W. Pan, Experimental twin-field quantum key distribution through sending or not sending, *Phys. Rev. Lett.* **123**, 100505 (2019).
- [49] X.-T. Fang, P. Zeng, H. Liu, M. Zou, W. Wu, Y.-L. Tang, Y.-J. Sheng, Y. Xiang, W. Zhang, H. Li, Z. Wang, L. You, M.-J. Li, H. Chen, Y.-A. Chen, Q. Zhang, C.-Z. Peng, X. Ma, T.-Y. Chen, and J.-W. Pan, Implementation of quantum key distribution surpassing the linear rate-transmittance bound, *Nat. Photonics* **14**, 422 (2020).

- [50] J.-P. Chen, C. Zhang, Y. Liu, C. Jiang, W. Zhang, X.-L. Hu, J.-Y. Guan, Z.-W. Yu, H. Xu, J. Lin, M.-J. Li, H. Chen, H. Li, L. You, Z. Wang, X.-B. Wang, Q. Zhang, and J.-W. Pan, Sending-or-not-sending with independent lasers: Secure twin-field quantum key distribution over 509 km, *Phys. Rev. Lett.* **124**, 070501 (2020).
- [51] H. Liu, C. Jiang, H.-T. Zhu, M. Zou, Z.-W. Yu, X.-L. Hu, H. Xu, S. Ma, Z. Han, J.-P. Chen, Y. Dai, S.-B. Tang, W. Zhang, H. Li, L. You, Z. Wang, Y. Hua, H. Hu, H. Zhang, F. Zhou, Q. Zhang, X.-B. Wang, T.-Y. Chen, and J.-W. Pan, Field test of twin-field quantum key distribution through sending-or-not-sending over 428 km, *Phys. Rev. Lett.* **126**, 250502 (2021).
- [52] X. Zhong, W. Wang, L. Qian, and H.-K. Lo, Proof-of-principle experimental demonstration of twin-field quantum key distribution over optical channels with asymmetric losses, *npj Quantum Inf.* **7** (2021).
- [53] J.-P. Chen, C. Zhang, C. Liu, Yang Jiang, W.-J. Zhang, Z.-Y. Han, S.-Z. Ma, X.-L. Hu, Y.-H. Li, F. Liu, Hui Zhou, H.-F. Jiang, H. Chen, Teng-Yun Li, L.-X. You, Z. Wang, X.-B. Wang, Q. Zhang, and J.-W. Pan, Twin-field quantum key distribution over a 511 km optical fibre linking two distant metropolitan areas, *Nat. Photonics* **15**, 570 (2021).
- [54] C. Clivati, A. Meda, S. Donadello, S. Virzi, M. Genovese, F. Levi, A. Mura, M. Pittaluga, Z. L. Yuan, A. J. Shields, M. Lucamarini, I. P. Degiovanni, and D. Calonico, Coherent phase transfer for real-world twin-field quantum key distribution, *arXiv preprint arXiv:2012.15199* (2020).
- [55] M. Pittaluga, M. Minder, M. Lucamarini, M. Sanzaro, R. I. Woodward, M.-J. Li, Z. Yuan, and A. J. Shields, 600-km repeater-like quantum communications with dual-band stabilization, *Nat. Photonics* (2021).
- [56] J.-P. Chen, C. Zhang, Y. Liu, C. Jiang, D.-F. Zhao, W.-J. Zhang, F.-X. Chen, H. Li, L.-X. You, Z. Wang, Y. Chen, X.-B. Wang, Q. Zhang, and J.-W. Pan, Quantum key distribution over 658 km fiber with distributed vibration sensing, *arXiv preprint arXiv:2110.11671* (2021).
- [57] L. Kazovsky, Balanced phase-locked loops for optical homodyne receivers: performance analysis, design considerations, and laser linewidth requirements, *J. Light. Technol.* **4**, 182 (1986).
- [58] L. G. Kazovsky and D. A. Atlas, A 1320-nm experimental optical phase-locked loop: performance investigation and psk homodyne experiments at 140 mb/s and 2 gb/s, *J. Light. Technol.* **8**, 1414 (1990).
- [59] K. Predehl, G. Grosche, S. M. F. Raupach, S. Droste, O. Terra, J. Alnis, T. Legero, T. W. Hänsch, T. Udem, R. Holzwarth, and H. Schnatz, A 920-kilometer optical fiber link for frequency metrology at the 19th decimal place, *Science* **336**, 441 (2012).
- [60] A. Huang, A. Navarrete, S.-H. Sun, P. Chaiwongkhot, M. Curty, and V. Makarov, Laser-seeding attack in quantum key distribution, *Phys. Rev. Applied* **12**, 064043 (2019).
- [61] X.-L. Pang, A.-L. Yang, C.-N. Zhang, J.-P. Dou, H. Li, J. Gao, and X.-M. Jin, Hacking quantum key distribution via injection locking, *Phys. Rev. Applied* **13**, 034008 (2020).
- [62] M. Lucamarini, I. Choi, M. B. Ward, J. F. Dynes, Z. L. Yuan, and A. J. Shields, Practical security bounds against the trojan-horse attack in quantum key distribution, *Phys. Rev. X* **5**, 031030 (2015).
- [63] S. Sajeed, A. Huang, S. Sun, F. Xu, V. Makarov, and M. Curty, Insecurity of detector-device-independent quantum key distribution, *Phys. Rev. Lett.* **117**, 250505 (2016).
- [64] G. Zhang, I. W. Primaatmaja, J. Y. Haw, X. Gong, C. Wang, and C. C. W. Lim, Securing practical quantum communication systems with optical power limiters, *PRX Quantum* **2**, 030304 (2021).
- [65] M. Bozzio, A. Cavallès, E. Diamanti, A. Kent, and D. Pitalúa-García, Multiphoton and side-channel attacks in mistrustful quantum cryptography, *PRX Quantum* **2**, 030338 (2021).
- [66] Y. Cao, Y.-H. Li, K.-X. Yang, Y.-F. Jiang, S.-L. Li, X.-L. Hu, M. Abulizi, C.-L. Li, W. Zhang, Q.-C. Sun, W.-Y. Liu, X. Jiang, S.-K. Liao, J.-G. Ren, H. Li, L. You, Z. Wang, J. Yin, C.-Y. Lu, X.-B. Wang, Q. Zhang, C.-Z. Peng, and J.-W. Pan, Long-distance free-space measurement-device-independent quantum key distribution, *Phys. Rev. Lett.* **125**, 260503 (2020).
- [67] H.-Y. Liu, X.-H. Tian, C. Gu, P. Fan, X. Ni, R. Yang, J.-N. Zhang, M. Hu, J. Guo, X. Cao, X. Hu, G. Zhao, Y.-Q. Lu, Y.-X. Gong, Z. Xie, and S.-N. Zhu, Optical-relayed entanglement distribution using drones as mobile nodes, *Phys. Rev. Lett.* **126**, 020503 (2021).
- [68] C.-Q. Hu, Z.-Q. Yan, J. Gao, Z.-M. Li, H. Zhou, J.-P. Dou, and X.-M. Jin, Decoy-state quantum key distribution over a long-distance high-loss air-water channel, *Phys. Rev. Applied* **15**, 024060 (2021).
- [69] Y.-A. Chen, Q. Zhang, T.-Y. Chen, W.-Q. Cai, S.-K. Liao, J. Zhang, K. Chen, J. Yin, J.-G. Ren, Z. Chen, *et al.*, An integrated space-to-ground quantum communication network over 4,600 kilometres, *Nature* **589**, 214 (2021).
- [70] D. Dequal, L. T. Vidarte, V. R. Rodriguez, G. Vallone, P. Villoresi, A. Leverrier, and E. Diamanti, Feasibility of satellite-to-ground continuous-variable quantum key distribution, *npj Quantum Inf.* **7**, 3 (2021).
- [71] J. Yin, Y.-H. Li, S.-K. Liao, M. Yang, Y. Cao, L. Zhang, J.-G. Ren, W.-Q. Cai, W.-Y. Liu, S.-L. Li, *et al.*, Entanglement-based secure quantum cryptography over 1,120 kilometres, *Nature* **582**, 501 (2020).
- [72] H. Takenaka, A. Carrasco-Casado, M. Fujiwara, M. Kitamura, M. Sasaki, and M. Toyoshima, Satellite-to-ground quantum-limited communication using a 50-kg-class microsatellite, *Nat. Photonics* **11**, 502 (2017).
- [73] S. Wehner, D. Elkouss, and R. Hanson, Quantum internet: A vision for the road ahead, *Science* **362**, eaam9288 (2018).
- [74] J. S. Sidhu, S. K. Joshi, M. Gündoğan, T. Brougham, D. Lowndes, L. Mazzarella, M. Krutzik, S. Mohapatra, D. Dequal, G. Vallone, P. Villoresi, A. Ling, T. Jennewein, M. Mohageg, J. G. Rarity, I. Fuentes, S. Pirandola, and D. K. L. Oi, Advances in space quantum communications, *IET Quantum Commun.* **2**, 182 (2021).
- [75] X. Ma and M. Razavi, Alternative schemes for measurement-device-independent quantum key distribution, *Phys. Rev. A* **86**, 062319 (2012).
- [76] S. Bose and D. Home, Duality in entanglement enabling a test of quantum indistinguishability unaffected by interactions, *Phys. Rev. Lett.* **110**, 140404 (2013).
- [77] Y.-M. Xie, C.-X. Weng, Y.-S. Lu, Y. Fu, Y. Wang, H.-L. Yin, and Z.-B. Chen, Scalable high-rate twin-field quantum key distribution networks without constraint of probability and intensity, *arXiv preprint*

- arXiv:2112.11165 (2021).
- [78] H. Xu, Z.-W. Yu, C. Jiang, X.-L. Hu, and X.-B. Wang, Sending-or-not-sending twin-field quantum key distribution: Breaking the direct transmission key rate, *Phys. Rev. A* **101**, 042330 (2020).
- [79] C. Jiang, X.-L. Hu, H. Xu, Z.-W. Yu, and X.-B. Wang, Zigzag approach to higher key rate of sending-or-not-sending twin field quantum key distribution with finite-key effects, *New J. Phys.* **22**, 053048 (2020).
- [80] K. Azuma, K. Tamaki, and W. J. Munro, All-photonics intercity quantum key distribution, *Nat. Commun.* **6**, 10171 (2015).
- [81] H.-K. Lo, X. Ma, and K. Chen, Decoy state quantum key distribution, *Phys. Rev. Lett.* **94**, 230504 (2005).
- [82] X.-B. Wang, Beating the photon-number-splitting attack in practical quantum cryptography, *Phys. Rev. Lett.* **94**, 230503 (2005).
- [83] H. Takesue, S. W. Nam, Q. Zhang, R. H. Hadfield, T. Honjo, K. Tamaki, and Y. Yamamoto, Quantum key distribution over a 40-dB channel loss using superconducting single-photon detectors, *Nat. Photonics* **1**, 343 (2007).
- [84] N. T. Islam, C. C. W. Lim, C. Cahall, J. Kim, and D. J. Gauthier, Provably secure and high-rate quantum key distribution with time-bin qudits, *Sci. Adv.* **3**, e1701491 (2017).
- [85] H. Chernoff, A measure of asymptotic efficiency for tests of a hypothesis based on the sum of observations, *Ann. Math. Stat.* **23**, 493 (1952).
- [86] H.-L. Yin, M.-G. Zhou, J. Gu, Y.-M. Xie, Y.-S. Lu, and Z.-B. Chen, Tight security bounds for decoy-state quantum key distribution, *Sci. Rep.* **10**, 14312 (2020).
- [87] H.-K. Lo and J. Preskill, Security of quantum key distribution using weak coherent states with nonrandom phases, *Quantum Inf. Comput.* **7**, 431 (2007).
- [88] M. Koashi, Simple security proof of quantum key distribution based on complementarity, *New J. Phys.* **11**, 045018 (2009).
- [89] H.-K. Lo, Proof of unconditional security of six-state quantum key distribution scheme, *Quantum Inf. Comput.* **1**, 81 (2001).
- [90] H.-L. Yin, Y. Fu, Y. Mao, and Z.-B. Chen, Security of quantum key distribution with multiphoton components, *Sci. Rep.* **6**, 29482 (2016).